Title
Cascading network failure across the Alzheimer's disease spectrum

Journal
Brain, 139(2)

ISSN
0006-8950

Authors
Jones, David T
Knopman, David S
Gunter, Jeffrey L
et al.

Publication Date
2016-02-01

DOI
10.1093/brain/awv338

Peer reviewed

doi:10.1093/brain/awv338 BRAIN 2016: 139; 547–562 | 547

BRAIN
A JOURNAL OF NEUROLOGY

Cascading network failure across the Alzheimer's disease spectrum

David T. Jones,[1,2] David S. Knopman,[1] Jeffrey L. Gunter,[2] Jonathan Graff-Radford,[1] Prashanthi Vemuri,[2] Bradley F. Boeve,[1] Ronald C. Petersen,[1] Michael W. Weiner[3] and Clifford R. Jack Jr[2] on behalf of the Alzheimer's Disease Neuroimaging Initiative*

*Data used in preparation of this article were obtained from the Alzheimer's Disease Neuroimaging Initiative (ADNI) database (adni.loni.usc.edu). As such, the investigators within the ADNI contributed to the design and implementation of ADNI and/or provided data but did not participate in analysis or writing of this report unless specifically listed above. A complete listing of ADNI investigators can be found at: https://adni.loni.usc.edu/wp-content/uploads/how_to_apply/ADNI_Acknowledgement_List.pdf.

Complex biological systems are organized across various spatiotemporal scales with particular scientific disciplines dedicated to the study of each scale (e.g. genetics, molecular biology and cognitive neuroscience). When considering disease pathophysiology, one must contemplate the scale at which the disease process is being observed and how these processes impact other levels of organization. Historically Alzheimer's disease has been viewed as a disease of abnormally aggregated proteins by pathologists and molecular biologists and a disease of clinical symptoms by neurologists and psychologists. Bridging the divide between these scales has been elusive, but the study of brain networks appears to be a pivotal inroad to accomplish this task. In this study, we were guided by an emerging systems-based conceptualization of Alzheimer's disease and investigated changes in brain networks across the disease spectrum. The default mode network has distinct subsystems with unique functional-anatomic connectivity, cognitive associations, and responses to Alzheimer's pathophysiology. These distinctions provide a window into the systems-level pathophysiology of Alzheimer's disease. Using clinical phenotyping, metadata, and multimodal neuroimaging data from the Alzheimer's Disease Neuroimaging Initiative, we characterized the pattern of default mode network subsystem connectivity changes across the entire disease spectrum ($n = 128$). The two main findings of this paper are (i) the posterior default mode network fails before measurable amyloid plaques and appears to initiate a connectivity cascade that continues throughout the disease spectrum; and (ii) high connectivity between the posterior default mode network and hubs of high connectivity (many located in the frontal lobe) is associated with amyloid accumulation. These findings support a system model best characterized by a cascading network failure—analogous to cascading failures seen in power grids triggered by local overloads proliferating to downstream nodes eventually leading to widespread power outages, or systems failures. The failure begins in the posterior default mode network, which then shifts processing burden to other systems containing prominent connectivity hubs. This model predicts a connectivity 'overload' that precedes structural and functional declines and recasts the interpretation of high connectivity from that of a positive compensatory phenomenon to that of a load-shifting process transiently serving a compensatory role. It is unknown whether this systems-level pathophysiology is the inciting event driving downstream molecular events related to synaptic activity embedded in these systems. Possible interpretations include that the molecular-level events drive the network failure, a pathological interaction between the network-level and the molecular-level, or other upstream factors are driving both.

1 Department of Neurology, Mayo Clinic, Rochester, MN, 55905, USA
2 Department of Radiology, Mayo Clinic, Rochester, MN, 55905, USA
3 Department of Veterans Affairs Medical Center, Center for Imaging of Neurodegenerative Diseases and Department of Radiology and Biomedical Imaging, University of California, San Francisco, CA, 94121, USA

Received April 13, 2015. Revised July 24, 2015. Accepted October 2, 2015. Advance Access publication November 19, 2015

Correspondence to: David T. Jones,
Mayo Clinic,
200 First Street S.W., Rochester,
MN 55905, USA
E-mail: jones.david@mayo.edu

Keywords: Alzheimer's disease; pathophysiology; cascading failure; complex systems; default mode network

Abbreviations: ADNI = Alzheimer's Disease Neuroimaging Initiative; DMN = default mode network

Introduction

Historically Alzheimer's disease has been viewed as a disease of abnormally aggregated proteins by pathologists and molecular biologists and a disease of clinical symptoms by neurologists and psychologists. A complimentary way to view the disease is through a pathological interaction between the microscale proteinopathy and macroscale brain networks leading to characteristic cascading failures that impart clinical symptomatology. The clinical course of a neurodegenerative disease is characterized by a progressive decline in specific cognitive functions over a period of years before involving more widespread cognitive functions. The progressive atrophy of a variety of neurodegenerative diseases takes place within specific large-scale brain systems, or intrinsic connectivity networks, unique to each disorder (Seeley *et al.*, 2009). These intrinsic connectivity networks are believed to support the diverse cognitive abilities observed to decline with disease progression. Put another way, network failure type imparts characteristic clinical phenotypes, or dementia syndromes. This is even true for phenotypic variability within disease states sharing the same underlying proteinopathy (Whitwell *et al.*, 2015).

Why do systems degenerate?

Several terms have been used to describe the predilection of neurodegenerative diseases to target large-scale brain networks [i.e. systems neurodegenerations (Saper *et al.*, 1987), network-based neurodegenerations (Greicius and Kimmel, 2012) and molecular nexopathies (Warren *et al.*, 2013)]. Theories attempting to explain the selective vulnerability of large-scale brain systems to neurodegenerative disease commonly invoke a molecularly driven conceptualization of the pathophysiology. These types of theories hold that aggregated misfolded proteins are the inciting event in neurodegenerative diseases, and explain the selective vulnerability of large-scale systems via a mechanism of prion-like spreading of these neurotoxic proteins along structural connections within brain networks (Raj *et al.*, 2012; Zhou *et al.*, 2012). However, as Zhou *et al.* (2012) have noted, these theories do not capture the 'complexity of [Alzheimer's disease] pathology which, in contrast to all other diseases studied…, features two co-occurring major molecular pathologies (amyloid-β and tau)'. On the other hand, it is also possible to espouse a systems-level conceptualization of neurodegenerative pathophysiology that designates the functional activity within large-scale brain networks as the consequence of the cellular changes, with those changes in functional activity being the driving force of both the expanding nature of the neurodegeneration and the clinical manifestations of the disease. Such a mechanism would predict system-level disruptions prior to characteristic spread of molecular pathology and naturally explain spatiotemporal gaps between molecular-level disease hallmarks (i.e. neurofibrillary tangles and amyloid plaques), given that distributed system-level changes do not require local physical proximity. It would also predict characteristic network disruptions heralding known patterns of clinical progression and neurodegeneration. However, these dynamic relationships are currently unknown, given that the spatiotemporal evolution of typical Alzheimer's disease-related large-scale brain system changes are not as clearly defined as the well-known sequence of clinical, molecular, structural, and metabolic changes seen with Alzheimer's disease (Jack *et al.*, 2013).

In the case of typical Alzheimer's disease, the pathophysiological process clinically manifests as a progressive amnestic syndrome (Dubois *et al.*, 2014). Given that typical Alzheimer's disease-related cognitive impairment interferes with the brain's ability to encode new memories, the large-scale systems affected in the typical Alzheimer's disease pathophysiologic cascade should also be implicated in the process of encoding new memories. The default mode network (DMN) was the first large-scale system shown to be disrupted in Alzheimer's disease (Greicius *et al.*, 2004). Other networks have since been implicated in Alzheimer's disease pathophysiology (Agosta *et al.*, 2012; Brier *et al.*, 2012). Atypical evolution of Alzheimer's disease pathophysiology beginning in non-memory systems (e.g. language, visual and executive systems) also involves similar networks, but these are not the topic of the current analysis.

DMN subsystems have distinct anatomical, functional and pathophysiological profiles

The DMN has not only been associated with memory but has also been implicated in other cognitive functions (Buckner *et al.*, 2008). Within this context, the DMN can be divided into subsystems more specifically associated with cognitive processes other than memory (Andrews-Hanna

et al., 2010; Raichle, 2015), and Alzheimer's disease has been demonstrated to affect these subsystems differently (Jones *et al.*, 2011). However, the extent to which these subsystems are affected in Alzheimer's disease may depend on the stage of the disease process (Damoiseaux *et al.*, 2012). An understanding of the differential temporal evolution of the Alzheimer's disease pathophysiological cascade within distinct DMN subsystems is a prerequisite to incorporating DMN metrics into biomarker models (Jack *et al.*, 2013) and for elucidating the mechanisms of the systems-level pathophysiology of Alzheimer's disease. A deeper understanding of the stages of the systems-level pathophysiology of Alzheimer's disease will allow for more informed investigations of the relationships between connectivity within distributed brain systems and molecular, cellular, and genetic levels of Alzheimer's disease pathophysiology.

In a seminal study by Andrews-Hanna *et al.* (2010), nodes within the DMN were shown to be segregated into three subsystems comprised of a midline core system containing both the posterior cingulate and anterior medial prefrontal cortex, a medial temporal lobe system, and dorsal medial prefrontal cortex system (Fig. 1A). These three subsystems were identified using graph-analytic and clustering analysis techniques applied to task-free functional MRI data extracted from *a priori* DMN seed regions. Using task-based functional MRI, these investigators demonstrated a functional dissociation of these subsystems. The midline core and the medial temporal lobe system were more associated with construction of mental scenes based on memory; however, the dorsal medial prefrontal cortex subsystem was more active when participants considered their present mental state and was more associated with affective self-referential processing.

Previous work by our group (Jones *et al.*, 2011) has shown that the pattern of connectivity changes in Alzheimer's disease dementia differ between these subsystem regions, with decreased DMN connectivity in the posterior cingulate and medial temporal lobe and increases found in medial prefrontal regions (Fig. 1B). In a subsequent study, we used high-dimensional group independent component analysis to isolate 31 intrinsic connectivity networks in a group of 892 cognitively normal older individuals (Jones *et al.*, 2012). Graph-analytic and clustering analysis applied to these data identified several subsystems within one module termed the task-negative network. Four of these DMN subsystems [i.e. ventral (vDMN), posterior (pDMN), anterior ventral (avDMN), and anterior dorsal (adDMN)] encompassed all of the regions of the DMN subsystems identified by Andrews-Hanna *et al.* (2010) (e.g. medial temporal lobe, posterior cingulate, anterior medial prefrontal, and dorsal medial prefrontal cortices, respectively; Fig. 1C). Using this functional brain parcellation, the dynamic connectivity was increased in Alzheimer's disease for anterior subsystems and decreased within posterior subsystems. However, how these connectivity changes progress across these subsystems at different points along the Alzheimer's disease spectrum is still unknown. Such information is imperative to understanding the systems-level pathophysiology of Alzheimer's disease and its temporal relationship to amyloid-beta and neurodegeneration, allowing unified understanding of disease pathophysiology at both macroscopic and microscopic scales.

Incorporating the systems-level pathophysiology into existing Alzheimer's disease models

In the current study, we used multimodal cross-sectional neuroimaging data from the Alzheimer's Disease Neuroimaging Initiative (ADNI) to investigate the evolution of connectivity changes within and between these four DMN subsystems across the Alzheimer's disease spectrum (see Supplementary Fig. 1 and Table 1 for patient selection and demographics, respectively). We first validate our novel connectivity measures in the ADNI dataset by demonstrating a relationship to out-of-scanner memory performance and replicate previous well-known findings comparing Alzheimer's disease dementia subjects to control subjects. Next, we characterized the pattern of DMN subsystem connectivity changes across the entire Alzheimer's disease spectrum and found a cascading network failure. This systems-level failure begins in the posterior DMN prior to any imaging evidence of spreading molecular pathology. These findings implicate the systems-level pathophysiology of Alzheimer's disease as an early event in Alzheimer's disease-related neurodegeneration and are potentially associated with amyloidosis via molecular events related to synaptic activity embedded in these systems. It remains an open question whether pathological synaptic activity within these systems precedes molecular events (Mesulam, 1999) or are purely a consequence of them (Spires-Jones and Hyman, 2014). Given that cascading failures are a common form of catastrophic failure in interdependent complex networks (Buldyrev *et al.*, 2010), we interpret the cascading network failure we observed in this study as evidence of a pathological interaction within complex systems composed of networks and molecules.

Materials and methods

Data used in the preparation of this article were obtained from the ADNI database (adni.loni.usc.edu). The ADNI was launched in 2003 by the National Institute on Aging, the National Institute of Biomedical Imaging and Bioengineering, the Food and Drug Administration, private pharmaceutical companies, and non-profit organizations as a $60 million, 5-year public–private partnership. The primary goal of ADNI has been to test whether serial MRI, PET, other biological markers, and clinical and neuropsychological assessment can be combined to measure the progression of mild cognitive impairment and early Alzheimer's disease. Determination of sensitive and specific markers of very early Alzheimer's disease progression is intended to aid researchers and clinicians to develop new treatments and monitor their effectiveness, as well as lessen the time and cost of clinical trials.

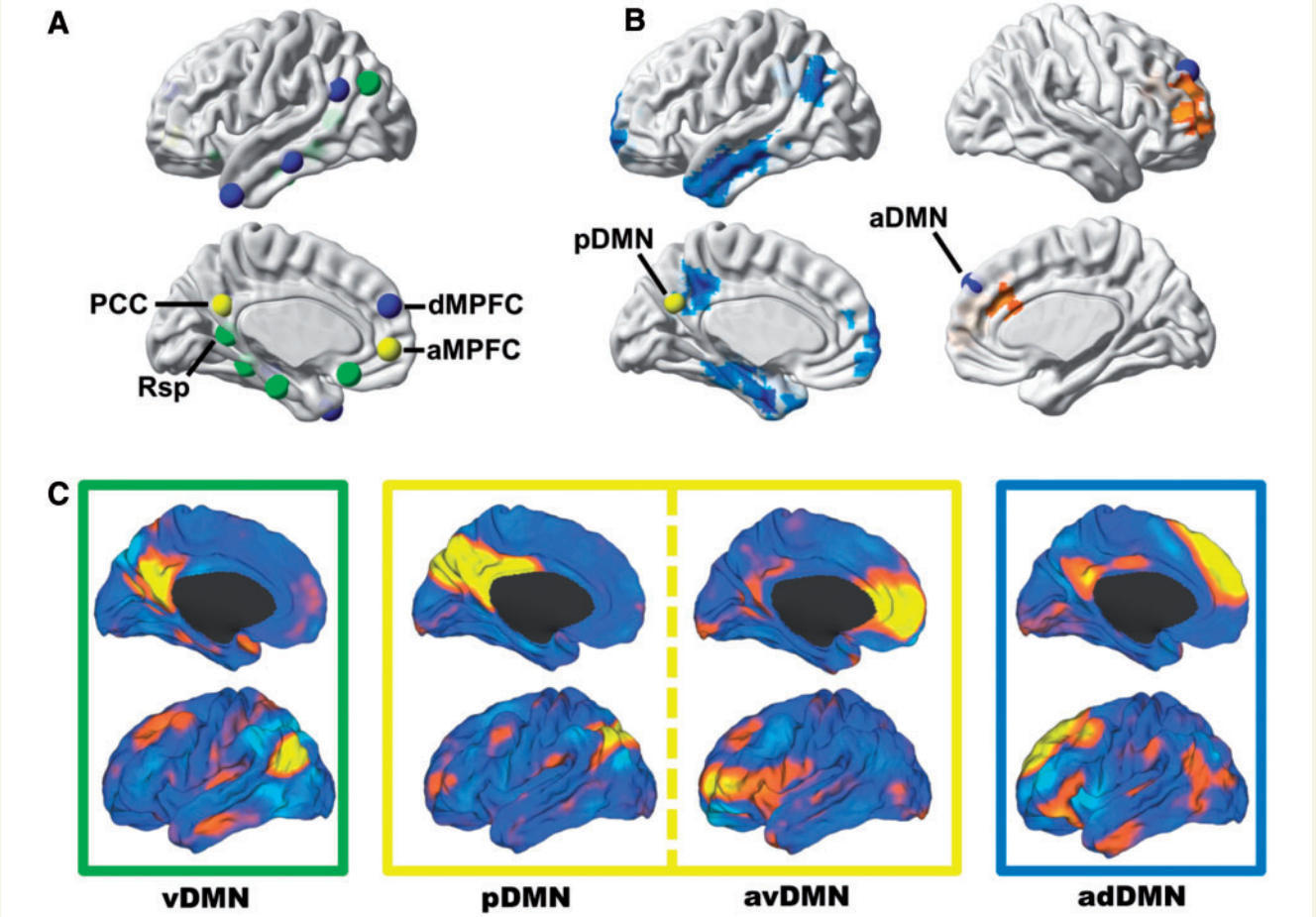

Figure 1 Subsystems of the DMN have distinct anatomical, functional, and pathophysiological profiles and can be isolated from one another in task-free functional MRI data. (**A**) Nodes within the DMN segregate into distinct subsystems, comprised of midline core regions (yellow), medial temporal lobe memory system (green), and a dorsal medial prefrontal cortex system (blue)—the regions and groupings were derived from Andrews-Hanna *et al.* (2010) and displayed on a cortical surface. (**B**) Seed-based analysis of posterior (left hemisphere) and anterior (right hemisphere) DMNs showing the divergent patterns of Alzheimer's disease dementia-related changes in connectivity in these subsystems (decreased in blue and increased in orange)—modified from Jones *et al.* (2011). (**C**) These same subsystems were identified in a high-dimensional GICA of intrinsic connectivity networks in a large (n = 892) population-based sampling of cognitively normal elderly participants in the Mayo Clinic Study of Aging (Jones *et al.*, 2012). The caret software package (Van Essen, 2005) was used to display these four independent components (i.e. ventral, posterior, anterior ventral, and anterior dorsal DMN) from this GICA analysis on brain surface renderings. Boxes around each of these renderings are colour coded to correspond to the subsystems nodes identified in **A** and **B**. aMPFC = anterior medial prefrontal cortex; dMPFC = dorsal medial prefrontal cortex; GICA = group independent component analysis; PCC = posterior cingulate cortex; Rsp = retrosplenial cingulate.

Participants

We identified all available task-free functional MRI scans in the ADNI database after baseline enrolment in ADNI-2 had been completed. If two task-free functional MRI studies were performed on the same day, the first scan was chosen unless it did not meet ADNI task-free functional MRI protocol standards or quality control measures. Defined in this manner, 636 ADNI task-free functional MRI studies were available for potential inclusion in this study. Sixty-four of these studies were excluded based on several factors: brain lesion confound (n = 2), subject exclusion from ADNI study (n = 1), uncertain clinical diagnosis (n = 2), structural image quality control failure (n = 1), overall task-free functional MRI quality control analyst rating >3 (on a scale of 1–4 with 1 being high quality and 4 being lowest quality) (n = 4), and any task-free functional MRI motion parameter exceeding 1.5 mm translation or 1.5° rotation (n = 55). Of the remaining 571 adequate quality studies, we defined the first available scan for each subject as the baseline scan to be included in this analysis (n = 204 unique baseline scans). If amyloid imaging was unavailable at the time of this study (n = 27), these subjects were not included in further analysis. All cognitively impaired subjects who were amyloid-negative were excluded from this analysis, as they are on a non-amyloid-related trajectory of cognitive impairment (Supplementary Fig. 1). Amyloid positivity was defined as suggested by ADNI methods document for cross-sectional florbetapir analysis using a cut-off of 1.11 using the whole cerebellum reference region, which is equivalent to the upper 95% confidence interval (CI) above the mean for a group of

Table 1 Subject demographics and metadata

	CN– *n* = 30	CN+ *n* = 13	SMC *n* = 7	EMCI *n* = 29	LMCI *n* = 21	AD-dementia *n* = 28	*P*-value
Age (Q1,Q3)	73 (68.5, 78)	73 (71, 79)	70 (67.5, 75)	71 (67, 74.5)	74 (71, 76)	74 (72, 76.5)	0.40
Male (%)	10 (33)	8 (62)	1 (14)	14 (48)	13 (62)	13 (46)	0.14
Education (Q1, Q3)	16 (16, 16)	16 (16, 18)	18 (14, 19.5)	16 (14, 18)	16 (16, 17.5)	15.5 (14, 16)	0.28
MMSE (Q1, Q3)	29 (28, 30)	29 (28, 30)	29 (29, 29)	28 (27, 29)	28 (26.5, 28)	22 (21, 25)	<0.001
CDR-SB (Q1, Q3)	0 (0, 0)	0 (0, 0)	0 (0, 0)	1.5 (1, 2)	2 (1.5, 2.5)	4.5 (4, 5)	<0.001
ADAS-Cog (Q1, Q3)	8 (6, 10.5)	9 (7, 10)	10 (9.5, 10)	12 (9, 17)	19 (14, 24)	32.5 (29, 40)	<0.001
AV-45 (Q1, Q3)	1.00 (0.97, 1.03)	1.39 (1.25, 1.47)	1.31 (1.27, 1.43)	1.34 (1.22, 1.43)	1.30 (1.25, 1.53)	1.46 (1.34, 1.58)	<0.001
aHV (Q1, Q3)	0.92 (0.12, 1.38)	−0.04 (−0.11, 1.11)	0.82 (0.43, 1.36)	0.58 (−0.12, 1.24)	0.1 (−0.71, 0.58)	−1.19 (−1.68, −0.15)	<0.001
APOE4 (%)	7 (23)	6 (46)	5 (71)	23 (79)	11 (52)	24 (86)	<0.001
FD_{max} (Q1, Q3)	0.81 (0.52, 1.02)	0.79 (0.55, 1.09)	0.71 (0.62, 1.24)	0.73 (0.59, 0.92)	0.83 (0.56, 1.00)	0.77 (0.63, 0.94)	0.95

AD = Alzheimer's disease dementia amyloid-positive; ADAS-Cog = 13-item Alzheimer's Disease Assessment Scale-Cognitive subscale; aHV = adjusted hippocampal volumes; AV-45 = florbetapir; CDR-SB = Clinical Dementia Rating Scale Sum of Boxes; CN – = cognitively normal amyloid-negative; CN + = cognitively normal amyloid-positive; EMCI = early mild cognitive impairment amyloid positive; FD_{max} = maximum frame-wise displacement; LMCI = late mild cognitive impairment amyloid positive; MMSE = Mini-Mental State Examination; SMC = significant memory concern amyloid-positive.

young normal control subjects (Joshi *et al.*, 2012). A complete list of the participants and images used is in Supplementary Table 1, with relevant metadata summarized in Table 1. Of note, there was no difference ($P = 0.95$) among clinical groups in maximum frame-wise displacement for the subject functional MRI scans included in this analysis [frame-wise displacement was calculated as described in Power *et al.* (2012)]. There was also no difference in proportion of any clinical category of subjects excluded during motion quality control ($P = 0.80$). There is a trend level correlation between increasing motion with advancing age ($r^2 = 0.022$, $P = 0.094$), but there is no difference in age between clinical groups ($P = 0.40$).

Structural MRI template for ADNI task-free functional MRI preprocessing

Because of the advanced age, ventricular size, and variable degree of atrophy among the elderly participants in this study, an out-of-sample template space based on young subjects is likely to have suboptimal sensitivity and localization of comparisons made between individuals in this cohort. Therefore, the gradwarp and biased corrected non-accelerated structural images of all available baseline scans were used to create a custom template for processing of task-free functional MRI data. The magnetization prepared rapid gradient echo (MP-RAGE) images used were acquired with no acceleration and a 1.2 mm right/left × 1 mm anterior/posterior × 1 mm superior/inferior reconstructed resolution. A repetition time/echo time of ∼7/3 ms was used. The ADNI protocols are publicly available on the adni.loni.usc.edu web site.

The structural template was created using the Diffeomorphic Anatomical Registration Through Exponentiated Lie Algebra (Ashburner, 2007) toolbox as implemented in SPM12 (http://www.fil.ion.ucl.ac.uk/spm/). This toolbox performs a high dimensional warping process that increases the registration between individuals, which results in improved localization and increased sensitivity in analyses. The entire baseline set of scans were initially segmented using the available SPM12 priors for six tissue classes (i.e. grey matter, white matter, CSF, bone, lipid, and air). These segmented images were then used to create the ADNI task-free functional MRI structural template space via the iterated non-linear registration procedure, producing increasingly crisp templates for each of these tissue classes. The manually-edited negative space of the union of the bone, lipid, and air template priors was used to define the intracranial volume of the template space. This template space with six tissue classes and intracranial volume (Supplementary Fig. 2) were used to processes all task-free functional MRI as outlined in the following section. The ADNI task-free functional MRI template is made freely available at http://mayoresearch.mayo.edu/mayo/research/jack_lab/supplement.cfm.

Task-free functional MRI preprocessing

The ADNI task-free functional MRI sequence is acquired with eyes open, single-shot gradient echo planar imaging on 3 T Philips MRI scanners with full brain coverage including the cerebellum with repetition time/echo time of 3000/30 ms, flip angle of 80°, 48 axial slices, a 64 × 64 in-plane acquisition matrix reconstructed to provide an isotropic 3.3 mm voxel size. The ADNI protocols, quality control information, and slice order information for each image is publicly available on the adni.loni.usc.edu website.

Given the importance of the order of operations in task-free functional MRI preprocessing, the preprocessing procedures are presented in the order in which they were performed (outlined in Supplementary Fig. 3). Conservatively, the first 10 volumes of the available 140 were removed to allow for steady state magnetization and avoid including the initial volumes, which tend to be more contaminated with artefact. Next, the time series within each voxel were despiked using AFNI's *3dDespike* program (http://afni.nimh.nih.gov). This process was done prior to realignment, given that realignment and motion correction may be improved by this despiking procedure (Jo *et al.*, 2013). Next, we performed slice-timing correction followed by two pass realignment to the mean echo planar image (EPI). The gradwarp and biased corrected non-accelerated structural images were then co-registered to the mean EPI image.

Unified segmentation and normalization to the ADNI task-free functional MRI template space was then performed. The

ADNI task-free functional MRI template space intracranial volume and the Mayo Clinic Study of Aging Functional Connectivity Atlas (Jones *et al.*, 2012) high-dimensional independent components of interest (i.e. ventral, posterior, anterior ventral and anterior dorsal DMN) were transformed to individual subject space using the inverse warps created during unified segmentation and normalization for each subject. To create an anatomically-based 'noise ROI' (region of interest) to be used in a component-based noise correction (Behzadi *et al.*, 2007) the subject space CSF and white matter segmentations were binarized at a 0.9 probability threshold and eroded by two voxels in each direction to avoid contamination with grey matter voxels. The union of the binarized and eroded images was used to extract the voxel-wise time-series to be used in a principal component analysis. The first six principal components were combined with the six motion parameters and their first temporal derivatives (18 total regressors) to create a nuisance regressor matrix to be used for further preprocessing.

Last, AFNI's *3dBandpass* program was used to detrend, simultaneously band-pass filter (0.009–0.08 Hz), and perform the nuisance regression using the nuisance regressor matrix. Simultaneous filtering and nuisance regression avoids spectral misspecification of motion artefact further reducing the impact of the motion confound (Hallquist *et al.*, 2013). This program was also used for time series variance normalization, masking, and smoothing with 6 mm full-width half-maximum Gaussian kernel.

Subject space spatial–temporal regression of DMN subsystems

Spatial independent component analyses applied to task-free functional MRI data identifies functionally connected brain networks in a data-driven fashion by estimating spatially-independent patterns from time courses of blood oxygenation level-dependent signal intensity. Group independent component analysis methods have been developed to draw inferences about group data using independent component analyses (Erhardt *et al.*, 2011). Subject-level maps may be back-reconstructed using the group-level solution to initialize a spatial-temporal regression procedure to estimate a subject-level solution (Filippini *et al.*, 2009). We have developed a well-characterized high-dimensional group independent component analysis atlas using a large population-based sampling of cognitively normal elderly individuals (Jones *et al.*, 2012). This out-of-sample atlas can be used to initialize the spatial-temporal regression method in a manner unbiased by the connectivity profiles of the sample of subjects under investigation.

For this study, the spatial–temporal regression was performed within a multivariate framework incorporating all four DMN subsystems of interest (i.e. posterior, ventral, anterior ventral, and anterior dorsal DMN) using functions from the GICA of functional MRI Toolbox (GIFT v2.0e) software package (Calhoun *et al.*, 2001), with scaling of the parameter estimates of functional connectivity to *z*-scores. The resulting spatial maps contain voxel-wise information about the spatial location and magnitude of functional connectivity at the individual subject level with corresponding temporal dynamics contained within the estimated time series for each DMN subsystem. Summary metrics for each of the network elements was then extracted from this result for each subject, obviating the need for voxel-wise comparison in standard space. Therefore, the spatial-temporal regression was performed in subject space to avoid potentially propagating any errors in the normalization process. In addition, the large spatial scale on which this procedure operates is theoretically robust to smaller scale variation in anatomy (e.g. gyration) or functional localization. To guard against potential bias related to differences in grey matter volume, spatial–temporal regression was performed within subject space incorporating only voxels with >0.5 probability of containing grey matter and excluding areas of signal loss (defined as mean signal intensity <100). This step, along with limiting our analysis to DMN subsystems, limits our summary metrics exposure to signal from brain regions with poor signal (see Supplementary Fig. 4 and discussion of limitations).

The within-subsystem connectivity (Supplementary Fig. 5A–D) was estimated by extracting the median value from the scaled spatial maps produced from the spatial-temporal regression procedure within a binarized region of interest consisting of the network template regions, which exceeded a z-score threshold of 7. The connectivity between DMN subsystems was estimated as the correlation between the four time courses produced during the spatial-temporal regression procedure (Supplementary Fig. 2A–F). The connectivity between the ventral DMN and the medial temporal lobe (Supplementary Fig. 2G) was estimated by extracting the median value from the scaled spatial map for the ventral DMN produced from the spatial-temporal regression procedure within the Automated Anatomic Labelling atlas (Tzourio-Mazoyer *et al.*, 2002) hippocampal region of interest.

Statistical procedures

A combination of MATLAB-based (Mathworks Inc., Natick, MA, USA) and R-based (http://www.R-project.org) software packages were used to perform all statistical analysis. A one-sample Kolmogorov-Smirnov test for normality was performed on each of the DMN elements investigated in this study. Strong evidence for non-normality was found (*P*-values ranging from 2.7×10^{-15} through 1.7×10^{-39}); therefore, testing of model assumptions was conducted where appropriate, and non-parametric statistical procedures were performed otherwise. Kruskal-Wallis one-way ANOVA was used for continuous variables, with *post hoc* Mann-Whitney U-tests for pair-wise differences. Friedman's test was used to test for differences in repeated measures. Chi-squared tests were used for categorical variables. When working within the generalized linear model framework using the Gaussian family distribution and an identity link function, we performed model diagnostics on the residuals (e.g. visualization of plots of jackknife residuals against linear predictor and normal scores plots of standardized deviance residuals) and found no compelling evidence to use alternative models. In our models of DMN subsystem response variables incorporating 13-item Alzheimer's Disease Assessment Scale-cognitive subscale and Clinical Dementia Rating Scale-sum of boxes as predictors while controlling for other confounding predictors, we investigated non-linearity within general additive models using penalized regression splines (Wood, 2006). We found similar functional forms with greater statistical significance using information theoretic criteria to select models (data not shown), but present the more rigorous generalized additive models in our results

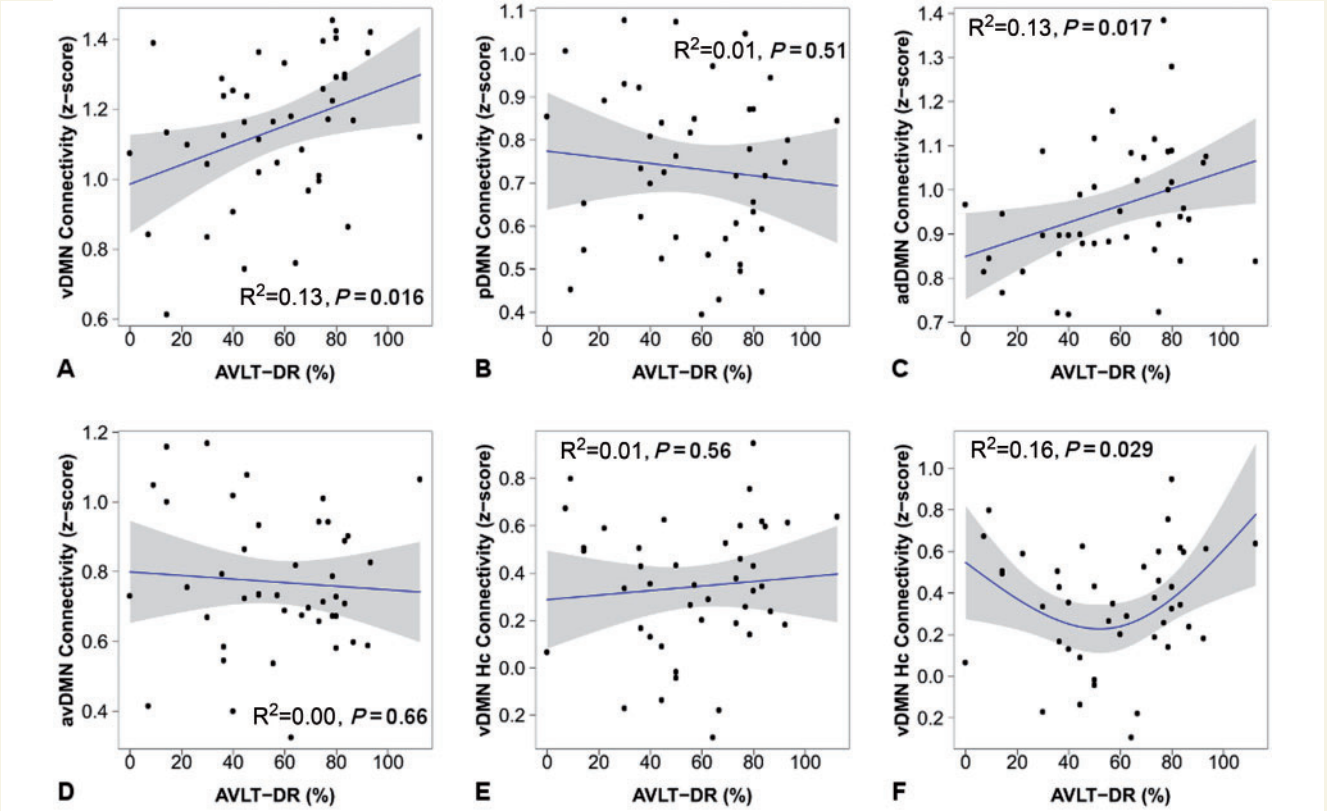

Figure 2 Connectivity measured during the 'resting state' is associated with out-of-scanner memory performance in cognitively normal participants ($n = 43$). The within-subsystem connectivity for each of the four DMN subsystems is plotted versus Rey Auditory Verbal Learning Test delayed recall (AVLT-DR) performance (**A–D**) and for ventral DMN hippocampal connectivity (Hc) versus AVLT-DR (**E** and **F**). Individual data points (black circles), regression lines (blue), and 95% confidence intervals (grey bands) are displayed for linear regressions (**A–E**) and for the second order natural spline non-linear regression (**F**).

section. A bootstrapping procedure was used to derive 95% CIs for each of these models. Non-linearity was similarly investigated in regression models of DMN subsystems connectivity and delayed recall portion of the Rey Auditory Verbal Learning Test.

Results

DMN subsystems, hippocampal connectivity and memory performance

The medial temporal lobe is a common target for connectivity biomarker development and plays a key role in Alzheimer's disease pathophysiology. Although there are variable reports as to hippocampal involvement in DMN intrinsic connectivity, Andrews-Hanna *et al.* (2010) solidly assign the medial temporal lobe to the subsystem we have termed the ventral DMN (*cf.* Fig. 1A and C). However, we empirically verified which subsystem has the strongest positive connectivity to the hippocampus to include in further analyses. Friedman's test was conducted across all available subjects in the study ($n = 128$) to compare hippocampal connectivity across the four DMN subsystems. There was a significant effect of DMN subsystems on observed hippocampal connectivity [$\chi^2(3,128) = 119.76$, $P < 0.001$] with the ventral DMN displaying the strongest connectivity with the hippocampus (Supplementary Fig. 6). Therefore, the ventral DMN connectivity with the hippocampus (Supplementary Fig. 5g) was included in all subsequent analyses.

Given the relationship between the medial temporal lobe and memory, the importance of memory to the earliest stages of the typical Alzheimer's disease clinical phenotype, and the relationship between the medial temporal lobe and the ventral DMN demonstrated here, we next investigated the relationship between intrinsic DMN subsystem connectivity and out-of-scanner memory performance. This exploratory analysis serves to better understand the distinct behaviour of these DMN subsystem elements, support nomenclature used, and also verify our assumption that they measure biologically relevant signal. We used a commonly used neuropsychological measure of memory performance in this clinical context (i.e. Rey Auditory Verbal Learning Test) in all cognitively normal subjects ($n = 43$). There was a significant linear correlation between ventral DMN connectivity and delayed recall performance ($r^2 = 0.13$, $P = 0.016$) and between anterior dorsal DMN connectivity

Table 2 Models of Alzheimer's disease dementia-related changes in DMN subsystems connectivity

Network Element[a]	Cohen's d	*P*-value[b]	*P*-value[c]
Ventral DMN (A)	**0.69**	**0.008**	**0.030**
Posterior DMN (B)	**0.80**	**0.002**	0.246
Anterior dorsal DMN (C)	−0.04	0.866	0.543
Anterior ventral DMN (D)	**−0.57**	**0.034**	0.210
Posterior and ventral DMN (a)	**−0.60**	**0.003**	**0.049**
Posterior and anterior dorsal DMN (b)	**−0.47**	**0.015**	**0.027**
Anterior dorsal and anterior ventral DMN (c)	0.08	0.589	0.899
Anterior ventral and ventral DMN (d)	0.24	0.336	0.669
Ventral and anterior dorsal DMN (e)	−0.01	0.808	0.739
Posterior and anterior ventral DMN (f)	0.05	0.878	0.984
Ventral DMN and MTL (g)	**0.54**	**0.024**	**0.046**

Results from the analysis comparing connectivity between Alzheimer's disease dementia subjects (n = 28) and cognitively normal subjects (n = 43) while controlling for motion, age, gender, and *APOE ε4* where indicated. *P*-values < 0.05 are in bold text.
[a]Upper case (A–D) and lower case (a–g) letters correspond to labels in Supplementary Fig. 5.
[b]Controlling for motion, age, and gender.
[c]Controlling for motion, age, gender, and *APOE ε4*.

and delayed recall performance (r^2 = 0.13, P = 0.017). No evidence was found for a linear relationship between posterior, anterior ventral, or ventral DMN hippocampal connectivity and delayed recall performance (Fig. 2). Additionally, no evidence for non-linear relationships was found except for a 'U-shaped' relationship between delayed recall performance and ventral DMN hippocampal connectivity (r^2 = 0.16, P = 0.029). This non-linear relationship is driven by the increase in ventral DMN hippocampal connectivity in the poorest memory performers, indicating that the phenomena of 'pseudonormalization' commonly observed in task functional MRI (Sperling *et al.*, 2010) is also present in task-free functional MRI. The term 'pseudonormalization' is used to denote a paradoxical rise in connectivity, or activation, in the poorest performers making them appear on par with normal performing subjects in terms of connectivity but not in terms of cognitive performance. This result validates our assumption that our measures of DMN subsystems relate to Alzheimer's disease-relevant cognitive abilities and is well inline with the existing task functional MRI literature (Sperling *et al.*, 2010).

Replication of Alzheimer's disease dementia-associated increases and decreases in DMN subsystem connectivity

Next, we sought to further validate our novel connectivity measures by replicating known Alzheimer's disease-related changes in DMN subsystems. We included the 28 subjects with Alzheimer's disease dementia with the 43 cognitively normal subjects and investigated group effects while controlling for motion, age, and gender. There was a significant difference in proportion of *APOE ε4* between these two groups, therefore significance of models with and without this term are presented in Table 2. These analyses revealed a pattern of Alzheimer's disease dementia-related increases and decreases in connectivity along a posterior–ventral to anterior–dorsal gradient. Significant Alzheimer's disease dementia-related decreases in connectivity were found for the ventral DMN and for the connection between the ventral DMN and the medial temporal lobe. A significant decrease in posterior DMN connectivity was seen with Alzheimer's disease dementia (P = 0.002), but significance was lost when *APOE ε4* was included in the model (P = 0.246). In contrast, the Alzheimer's disease dementia-related decline in ventral DMN connectivity was significant whether *APOE ε4* was included in the model (P = 0.030) or not (P = 0.008).

Alzheimer's dementia related increases in connectivity were found within the anterior ventral DMN and in the connections between the posterior and the ventral DMN and between the posterior and the anterior dorsal DMN.

DMN subsystems have distinct functional forms across the Alzheimer's disease-spectrum

To investigate how each of the Alzheimer's disease-related DMN subsystem elements found to be abnormal in Alzheimer's disease dementia (Table 2) changed as a function of disease severity, we included all of the available subjects on the Alzheimer's disease pathophysiological spectrum (n = 128), excluding the subjects who were amyloid negative and clinically impaired, as they were not on this spectrum and were unlikely to display an Alzheimer's disease pattern of change in DMN connectivity (Supplementary Fig. 1). These cross-sectional functional forms delineate the pattern of association between DMN subsystems and clinical progression from preclinical to dementia while controlling for motion, age, gender, and

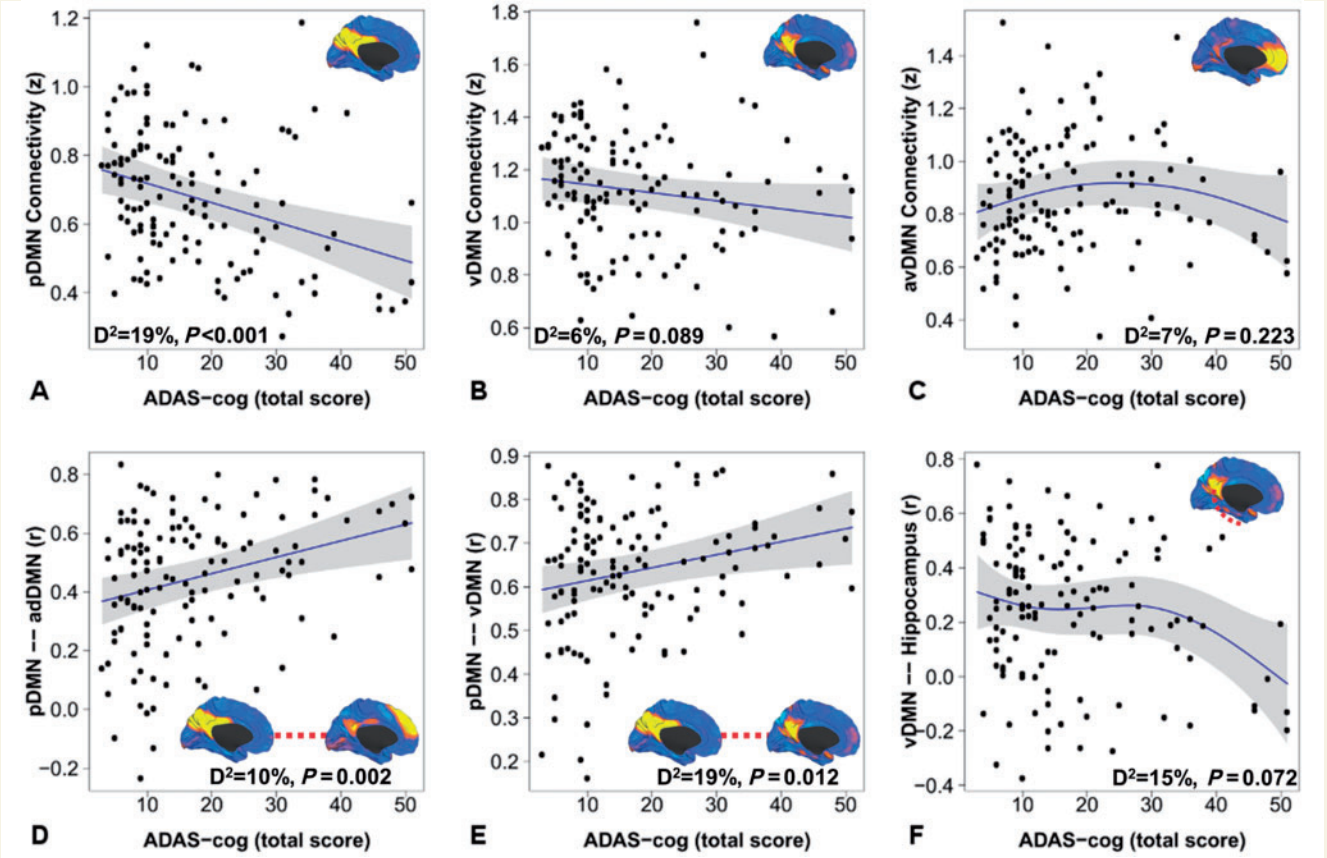

Figure 3 DMN subsystem elements have distinct functional forms in their association with progression along the Alzheimer's disease spectrum. The within-subsystem connectivity for the posterior DMN (**A**), ventral DMN (**B**), and anterior ventral DMN (**C**) is plotted versus raw score on the 13-item Alzheimer's Disease Assessment Scale-cognitive subscale within generalized additive models controlling for motion, age, gender, and *APOE ε4*. The medial surface topography for within-subsystem connectivity is inset for **A–C**. Similar plots are made for significant between-subsystem elements (**D** and **E**) and ventral DMN to hippocampal connectivity (**F**). The deviance explained by the models and *P*-value for each element displayed is inset. Individual data points (black circles), regression lines (blue), and 95% CIs (grey bands) are displayed. Identical functional forms were obtained replacing 13-item Alzheimer's Disease Assessment Scale-cognitive subscale with the Clinical Dementia Rating Scale-sum of boxes (data not shown).

APOE ε4 carriage. Similar functional forms were found whether we used the 13-item Alzheimer's Disease Assessment Scale-cognitive subscale (Fig. 3) or Clinical Dementia Rating Scale-sum of boxes (data not shown) as an index of disease progression.

The within subsystem posterior DMN and ventral DMN decline linearly throughout the disease course (Fig. 3A and B), while the connections between the posterior and the ventral DMN, and between the posterior and the anterior dorsal DMN, linearly increase (Fig. 3D and E) throughout the disease course. When viewed across the entire spectrum of the disease, the increase in anterior ventral DMN connectivity in the Alzheimer's disease dementia model (Table 2) appears to have a trend towards declining levels of connectivity after the initial increase in the early disease phases (Fig. 3C). The decline in ventral DMN connectivity with the hippocampus also appears to take a non-linear trajectory across the disease course (Fig. 3F) within generalized additive models. Similar functional forms with greater statistical significance are found when AIC minimization is used to define model order (data not shown).

Connectivity, hippocampal volume and amyloid levels

To visualize these network level patterns of pathological change in the context of more well-known patterns of biomarkers of molecular pathological changes, we performed the same analyses across the disease spectrum using amyloid-PET and hippocampal volume (Fig. 4A and B). The functional forms of all of these levels of Alzheimer's disease pathophysiology are then overlaid for visual comparison (Fig. 4C). In direct comparison, declining posterior DMN connectivity (controlling for motion, age, gender, and

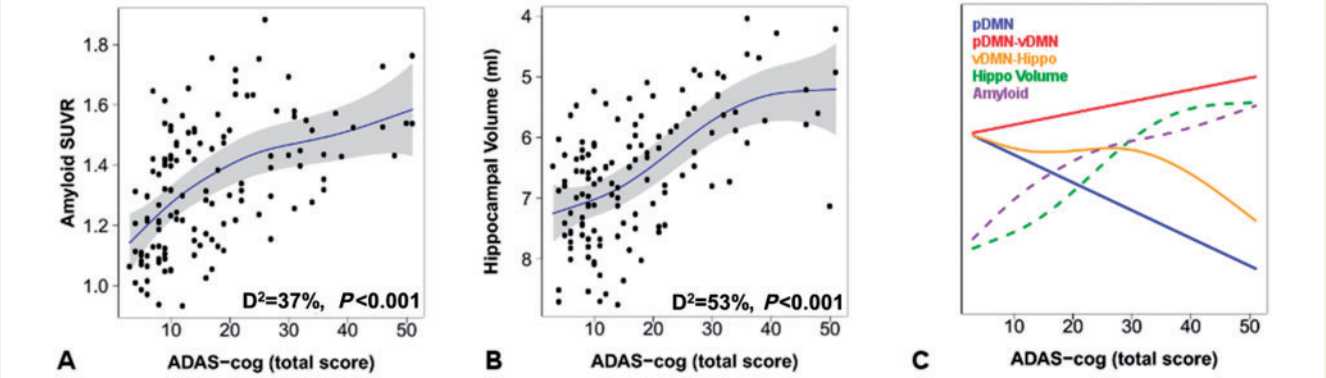

Figure 4 Incorporating network changes into models of the molecular- and cellular-level changes across the Alzheimer's disease spectrum. Amyloid-PET (**A**) and hippocampal volume (**B**) are plotted versus raw score on the 13-item Alzheimer's Disease Assessment Scale-cognitive subscale within generalized additive models controlling for age, gender, *APOE ε4*, and total intracranial volume (hippocampal volume only). The deviance explained by the models and *P*-value for each element displayed is inset. Individual data points (black circles), regression lines (blue), and 95% CIs (grey bands) are displayed. The same analysis performed for network elements (blue, gold, and red solid lines for the posterior DMN, posterior to ventral DMN connection, and ventral DMN to hippocampal connection, respectively) are plotted with amyloid-PET (purple dotted line) and hippocampal volume (green dotted line) (**C**). For clarity, the 95% CIs are omitted, but can be inspected in the plots for each element individually (see Figs 3A, E, F, 4A and B).

APOE ε4) is marginally associated with elevated amyloid levels ($\beta = -0.15$, $P = 0.08$), but is not associated with hippocampal volume ($P = 0.54$). However, the increasing connection between the posterior and the ventral DMN is associated both with elevated amyloid levels ($\beta = 0.23$, $P = 0.009$) and declining hippocampal volume ($\beta = -0.17$, $P = 0.03$). In fact, the within posterior DMN connectivity is no longer associated with amyloid levels when the connection between the posterior and the ventral DMN is controlled for ($\beta = -0.09$, $P = 0.35$), but the association between higher levels of posterior to ventral DMN connectivity and higher amyloid levels remains significant ($\beta = 0.20$, $P = 0.034$).

Low posterior DMN connectivity and absent amyloid, hippocampal, and ventral DMN changes in cognitively normal *APOE ε4* carriers

To isolate the earliest possible changes in these biomarkers of Alzheimer's disease, we looked at *APOE ε4*-related differences in cognitively normal subjects who were amyloid-negative (Fig. 5). Carriage of the *APOE ε4* allele (controlling for age, gender, and motion) was associated with lower posterior DMN connectivity ($\beta = -0.50$, $P = 0.008$), but not with differences in ventral DMN connectivity ($\beta = 0.21$, $P = 0.26$), connectivity between the posterior and the ventral DMN ($\beta = 0.01$, $P = 0.98$), or hippocampal volume ($\beta = 0.13$, $P = 0.45$).

These findings combined with the results above imply a strong effect of *APOE ε4* carriage on posterior DMN connectivity independent of amyloid pathology and Alzheimer's disease dementia. These findings alone do not implicate posterior DMN failure as the earliest critical event in Alzheimer's disease pathophysiology. They are, however, strongly supportive of this interpretation when taken in the context of the other results of this study and the existing longitudinal literature (see 'Discussion' section).

Discussion

Cross-sectional connectivity changes across the Alzheimer's disease spectrum

Typical Alzheimer's disease follows a stereotypical pattern of cognitive impairment, beginning first with the encoding of new memories and inevitably progressing to involve diverse cognitive faculties (Petersen, 2003). This typical amnestic clinical syndrome has been associated with a characteristic topographic spread of molecular pathology (Braak and Braak, 1991; Thal *et al.*, 2002), progressive atrophy of the medial temporal lobe prior to atrophy of the temporoparietal and frontal regions (Scahill *et al.*, 2002), and early metabolic derangements in the posterior cingulate and lateral temporoparietal regions prior to involving frontal regions (Minoshima *et al.*, 1997). These pivotal cross-sectional studies defined the characteristic stages of the molecular, cellular and metabolic changes associated with the progression of Alzheimer's disease; however, there has been no such cross-sectional description of the progressive network changes in Alzheimer's disease. Herein, we report that the systems-level pathophysiology of Alzheimer's disease appears to spread across DMN

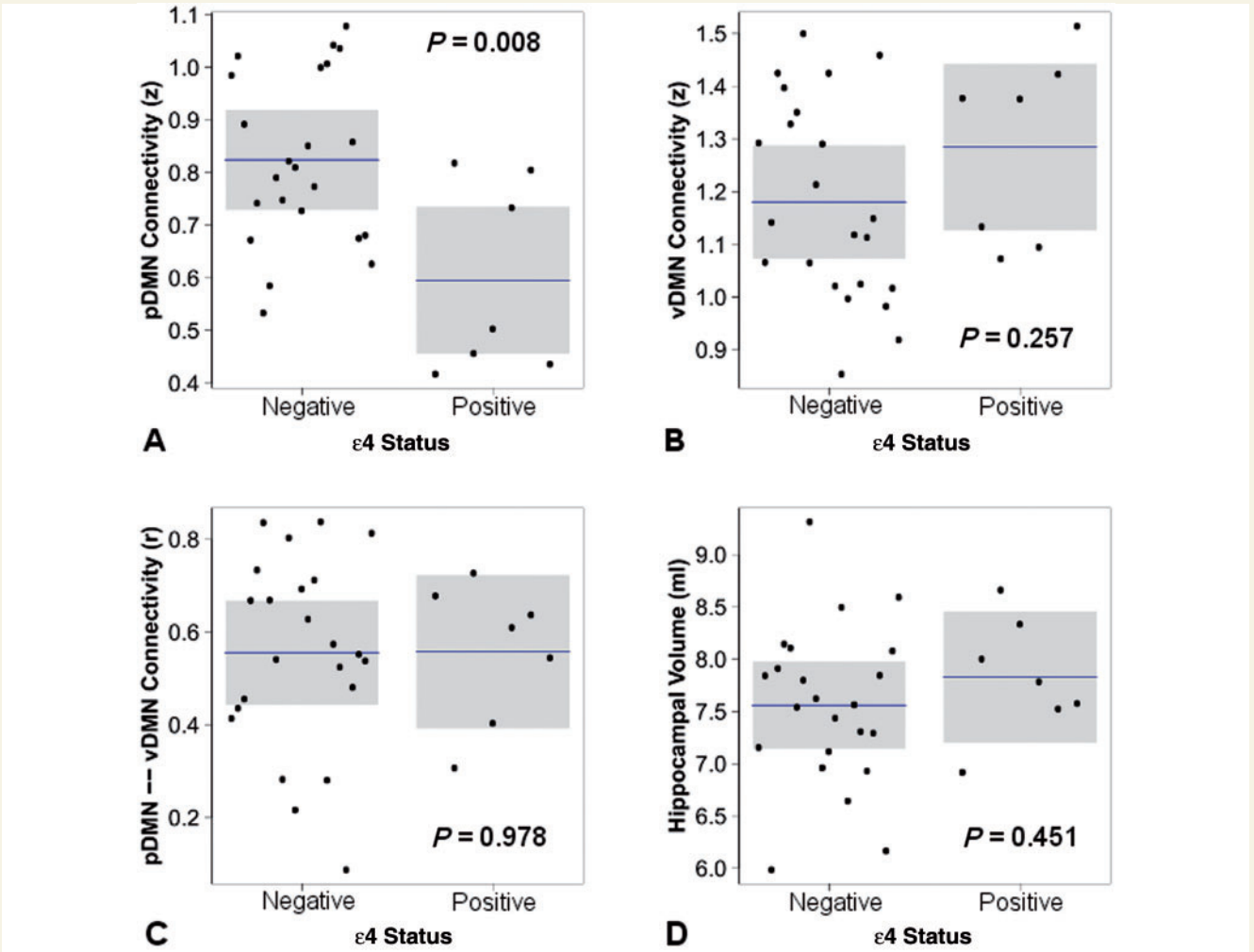

Figure 5 The effect of *APOE ε4* carriage in cognitively normal subjects without evidence of amyloid plaques. The response variable is plotted with mean and 95% CIs by *APOE ε4* status holding all other variable constant including age, gender, motion (**A–C** only) and total intracranial volume (**D** only).

subsystems in a manner consistent with a cascading network failure that begins with a decline in the most highly connected posterior brain regions and progresses via sequential increases in connectivity across a posterior-ventral to anterior-dorsal gradient (Fig. 3), mirroring the known spatiotemporal patterns of involvement in these other markers of Alzheimer's disease-pathophysiology.

Using our analysis of the patterns of connectivity across the pathophysiological spectrum (operationally defined here as a combination of clinical deficit plus the presence of amyloidosis on PET), there were three major themes that emerged. First, dysfunction in the medial temporal lobe-ventral DMN pathway was associated with dysfunction in memory. Second, the connectivity analysis demonstrates the interactions/interrelationships between posterior and ventral DMN in the form of increased connectivity between the two as cognition declined. In fact, the connectivity increase between the two reflects disease severity as measured by clinical indicators of impairment. In addition, this increased connectivity is also associated with imaging markers of disease progression (i.e. increasing amyloid PET signal and declining hippocampal volume). This is in contrast to the posterior DMN, which showed declining connectivity as a function of disease severity, but is unassociated to amyloid and hippocampal volume. Third, carriage of *APOE ε4* allele had a specific relationship to the posterior DMN that was evident in cognitively normal subjects before any other system or molecular level change could be measured.

Network failure begins in the posterior DMN and cascades through the brain via increased connectivity (overload)

In amyloid-negative at-risk individuals, i.e. *APOE ε4* allele carriers, we observed decreased connectivity within the posterior DMN but no difference in connectivity in the ventral DMN or in the connectivity between the posterior and the ventral DMN. As the within-posterior DMN connectivity lowers in later disease stages, it is still not associated with

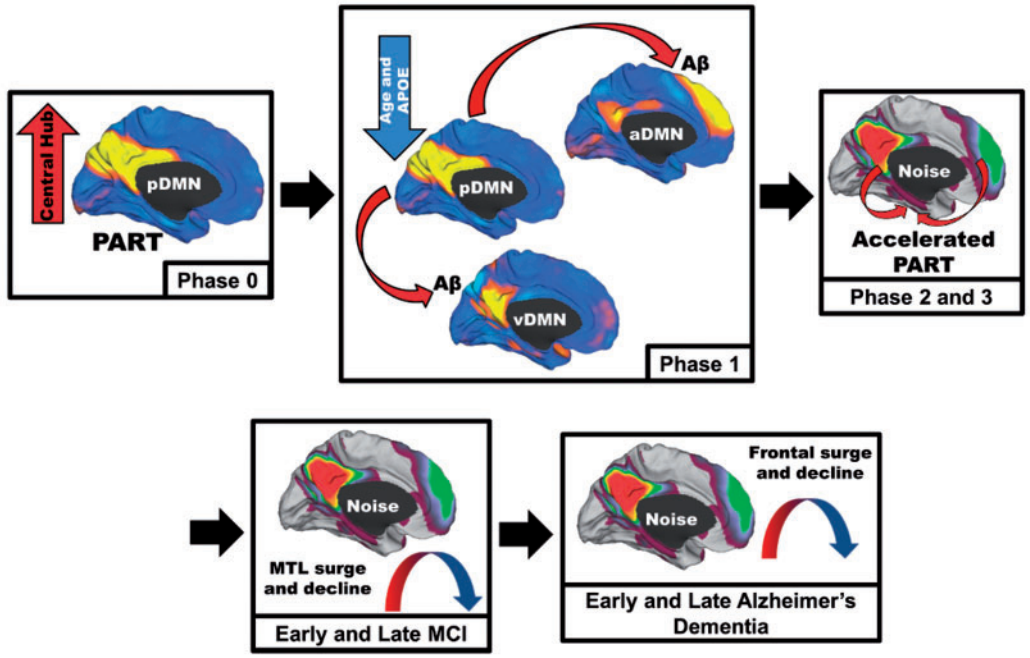

Figure 6 Schematic of the proposed cascading network failure model of Alzheimer's disease. Phase 0: The posterior DMN (pDMN) serves as the central hub processing and integrating association cortices and is highly metabolically active. Independently, the medial temporal lobe (MTL) has accumulated age-related damage from neocortical processing of a different kind (pattern separation and completion) contributing to primary age-related tauopathy (PART) in these regions. Phase 1: The declining posterior DMN (Fig. 3A), more prominent with advancing age and *APOE ε4* carriage, transfers information processing duties (or starts passing noisy signals) to the neocortical regions including the ventral DMN (Fig. 3D) and/or the anterior dorsal DMN (Fig. 3E). Aberrant between-neocortical network synaptic activity leads to dysregulated amyloid precursor protein (APP) processing promoting amyloid-β (Aβ) plaque formation in neocortical layers. Phase 2: Given that the hippocampus is continually processing information from these same regions, noise in these cortical systems is propagated down to the hippocampus. This increased burden on the hippocampus accelerates the pre-existing PART. Phase 3: Neurodegeneration expands to adjacent systems. This creates a detrimental positive feedback loop because degeneration lowers the noise handling capacity of the system leading to further degeneration. MCI Phase: Posterior brain regions supporting memory succumb to the degenerative feedback loop as hippocampal regions increase processing (Fig. 3F). Later the frontal brain regions begin to bear the high connectivity burden (Fig. 3C). Early Alzheimer's disease phase: The high frontal connectivity firmly establishes the neurodegenerative feed-back loop in these systems before declining as Alzheimer's disease progresses.

amyloid or hippocampal volume when controlling for high connectivity between the posterior and ventral DMN. This suggests that there is a within subsystems decline in the posterior DMN followed by a transient compensatory increase in connectivity between the posterior DMN and other systems that are associated with amyloid and hippocampal volume. A longitudinal study of DMN subnetworks found a similar pattern of a posterior DMN decline in contrast to an initially increased connectivity within the ventral and anterior DMN, both subsequently declining along with the posterior DMN during longitudinal follow-up (Damoiseaux *et al.*, 2012). These commonly observed increases in connectivity have typically been interpreted to represent a compensatory phenomenon (Mormino *et al.*, 2011). However, we hypothesize that the metabolic demands associated with high connectivity may be the detrimental phenomenon that triggers downstream cellular and molecular events associated with Alzheimer's disease. High connectivity may be a sign of high processing burden and/or noisy inefficient synaptic communication. This processing burden may then be shifted, or inefficient noisy communication may be propagated, to downstream areas within highly-connected networks. This proposed process of a cascading network failure (see Fig. 6 for details) propagated by surges in activity, is analogous to cascading failures seen in power grids triggered by local overloads proliferating to downstream nodes eventually leading to widespread power outages, or systems failures. The shifting of processing burden to downstream elements may also be conceptualized as a compensatory process supporting better performance on cognitive tasks (Elman *et al.*, 2014), albeit a compensatory strategy that may eventually lead to widespread system failure. A systems conceptualization of these processes shifts explanations of resilience to microscopic pathological burden (Perez-Nievas *et al.*, 2013) to explanations of robustness of networks to cascading failures—a paradigm ideally suited to theories involving the effects of a life-time of cognitive activity (Iacono *et al.*, 2009; Jagust and Mormino, 2011) on large-scale network topology.

Connectivity, selective vulnerability, and amyloid

Thinking about Alzheimer's disease in connectivity terms is a natural endeavour given the long-known peculiar predilection of the disease for posterior isocortical association areas, and is supported by the recent descriptions of the mechanisms of trans-synaptic spread of misfolded proteins. Our empiric observations are consistent with the theoretical framework of a cascading network failure wherein dysfunction that begins in one region leads to increased connectivity within the DMN, which further strains the synaptic and cellular machinery. It may be that this interaction between the global systems-level and a local brain region/system with vulnerable molecular substrates (e.g. aggregated misfolded proteins) is the pathophysiological process that leads to stereotypic network-based neurodegenerative clinical syndromes. Variable clinical syndromes (e.g. typical amnestic versus language variants) may be related to the pattern of interaction between networks and pre-existing vulnerable molecular/cellular substrates in particular brain regions—the most common substrate/region being primary age-related tauopathy in the medial temporal lobe (Crary *et al.*, 2014). In this respect, in may be that amyloidosis is related to the system failure in general and not the particular pattern of interaction between networks and vulnerable brain regions. Our recent work comparing network dysfunction in typical amnestic and language variants of Alzheimer's disease is consistent with this interpretation (Whitwell *et al.*, 2015). This interpretation is also supported by the fact that amyloidosis largely follows a homogeneous spatial distribution that is highly associated with connectivity hubs (Buckner *et al.*, 2009), yet regions of neurodegeneration and clinical presentations are much more variable (Warren *et al.*, 2012).

While the causal relationship between the observed affiliation between amyloid-β and this network failure remains unclear, we have made several observations that inform a discussion of this association. These Alzheimer's disease-related systems-level changes (Table 2) are occurring within the context of similar age-related changes in DMN subsystems (Jones *et al.*, 2011). The *APOE ε4* effect enhances these changes most markedly in the posterior DMN prior to measurable amyloid deposition (Fig. 5), suggesting that the posterior DMN decline related to ageing and the initiation of Alzheimer's disease-related network failure may be a more proximate event than amyloid accumulation currently measurable *in vivo*. These results are consistent with our previous finding (Machulda *et al.*, 2011) of an *APOE ε4*-related decline in posterior DMN connectivity in cognitively normal elderly and also that this occurs in *APOE ε4* allele carriers who are documented to be amyloid-negative, as previously reported by others (Sheline *et al.*, 2010). In addition, the brain regions within the posterior DMN largely overlap with the areas of the brain that have a unique vulnerability to reductions in glucose metabolism as a function of both age and *APOE ε4* allele carriage, which are also independent of amyloid status (Jagust and Landau, 2012; Knopman *et al.*, 2014). These findings imply that the function of the posterior DMN is impaired during ageing, and to a greater degree in asymptomatic *APOE ε4* allele carriers, and then continues to further decline during Alzheimer's dementia. This preclinical disruption is accompanied by a decline in connectivity and metabolic derangements before measurable amyloid accumulation. These findings highlight functional-metabolic coupling within these brain regions and suggest a potential vulnerability to cascading failures within interdependent networks experiencing high processing demands (Buldyrev *et al.*, 2010), and this vulnerability appears to be independent of amyloid status.

Further, we observed no relationship between declining within posterior DMN connectivity and amyloid PET when controlling for high connectivity between the posterior and the ventral DMN. This indicates that measurable amyloid-β does not drive the within-posterior DMN decline, but it is associated with high connectivity between the posterior and the ventral DMN. Combining these observations with the *APOE ε4*-related decline in posterior DMN connectivity and the observed Alzheimer's disease-related cascading network failure (hypothesized to originate in the posterior DMN), implicates the systems-pathology, or the interaction of the network-level with the molecular level (e.g. synaptic amyloid-β precursor protein processing is increased with increased/noisy network signalling), as a candidate proximate cause of amyloidosis. We acknowledge that this is just one possible interpretation; with others being that the amyloid plaques cause the network-level disruption, or other factors drive both the amyloid plaques and network-level changes. Chief among these other potential factors would be forms of amyloid not captured by PET imaging. We cannot comment on the apparent temporal relationships with subthreshold amyloid deposition or soluble amyloid species. However, if these subthreshold amyloid-related events were the driving force behind the observed network-level changes, then this effect should be observable at suprathreshold amyloid levels as well. Consequently, causative amyloid-related effects would manifest in some statistical relationship between detectable amyloid and these relevant posterior DMN changes in the preclinical disease phase; however, we did not observe such a relationship, although, such a relationship has been reported using other measures of connectivity focused on the medial temporal lobe (Song *et al.*, 2015).

Implications for using connectivity as a biomarker

The ADNI cohort used in this analysis represents a population of subjects in which potential biomarkers can be tested for use in clinical trials, and this DMN-focused investigation has important implications in this regard. If

DMN connectivity is to be used either as a stratification or outcome variable in clinical trials, then the differential involvement of DMN subsystems and the non-linear trajectories demonstrated here must be taken into consideration. In addition, the variance explained by these functional forms using current acquisition and analyses methods is still small. However, as more cutting-edge techniques become applicable to this patient population [e.g. via dissemination of advances made by the Human Connectome Project (Ugurbil *et al.*, 2013)], connectivity biomarker development should consider these functional forms and the cascading network failure they suggest. In this regard, multivariate isolation of early declines in parietal regions of the posterior and ventral DMN appear attractive, as these may track linearly with disease progression. It should be emphasized, however, that the declines in 'within-DMN subsystems' changes must be isolated, or the measurement will be contaminated with linear increases in 'between-subsystem' connectivity (Fig. 3D and E).

This is in contrast to hippocampal (Figs 2F and 3F) and frontal (Fig. 3C) contributions to DMN connectivity, where the bulk of the non-linearity was observed in this study. As Sperling *et al.* (2010) have emphasized, the problem of 'pseudonormalization' will have to be dealt with before such non-linear trajectories can be leveraged as useful biomarkers. Isolating different DMN subsystems to focus on the biological changes and functional forms of interest will require the application of multivariate approaches. In general, the non-stationarity in brain dynamics (Jones *et al.*, 2012) and non-linearity in Alzheimer's disease-related changes in network connectivity indicate that the study of network-based neurodegeneration must increasingly rely on the tools afforded by the continuously emerging field of complex adaptive systems, e.g. analyses of complex networks (Bullmore and Sporns, 2009), to make meaningful advances. A well developed complex systems-based understanding of Alzheimer's disease pathophysiology will open up new avenues for therapeutic interventions targeting large-scale brain dynamics in preclinical Alzheimer's disease.

Limitations

An important limitation in the ADNI task-free functional MRI dataset should be made clear. While functional MRI signal loss related to susceptibility artefacts is a common problem affecting brain regions near the skull base, in the ADNI data, the left lateral frontal lobe tends to be affected by a 'penciling artefact' that also decreases functional MRI signal in this region (Supplementary Fig. 4). It is uncertain how this might affect connectivity analyses including this region; we have therefore carefully avoided this region in our DMN metrics. Additionally, this study has several limitations inherent in cross-sectional designs and large multicentre studies. However, as multimodal longitudinal data continue to accrue through ADNI, follow-up studies investigating DMN subsystem evolution across the Alzheimer's disease spectrum will be possible. Such studies will be able to test the cascading network failure hypothesis presented here. To this end, all of the DMN subsystem metrics, ADNI template space priors, and multimodal neuroimaging data used in this paper are available for download from the ADNI website (http://adni.loni.usc.edu).

Conclusion

We propose a cascading network failure mechanism (Fig. 6) to explain our connectivity findings across the Alzheimer's spectrum but acknowledge that other interpretations are certainly plausible and have been widely discussed in the extant literature and therefore not discussed in more detail here. This model proposes that a key event in the development of Alzheimer's disease is when the posterior DMN fails and begins shifting processing burden to other hub brain regions. Synaptic events within connectivity hubs related to this shifting of processing burden leads to aberrant amyloid-β precursor protein processing and amyloidosis. At this stage, systemic and synaptic homeostatic responses may have the potential to avert the cascading failure before it is able to interact with vulnerable brain regions. However, in the case of typical Alzheimer's disease, the cascading network failure interacts with a pre-existing vulnerable substrate in the medial temporal lobe, recently termed primary age-related tauopathy (Crary *et al.*, 2014). This interaction leads to, or accelerates, a progressive tau-associated neurodegenerative process involving a stereotypical sequence of brain regions and observed clinical features.

Acknowledgements

We would like to thank Bret Borowski, Denise Reyes, Heather Wiste, and Brain Gregg for their work on data management and quality control. We would also like to thank Joe Fleming of Joe Motion (www.joemotion.tv) for invaluable assistance with thumbnails and cover art.

Funding

Data collection and sharing for this project was funded by the Alzheimer's Disease Neuroimaging Initiative (ADNI) (National Institutes of Health Grant U01 AG024904) and DOD ADNI (Department of Defense award number W81XWH-12-2-0012). Additional funding for this study was provided by the National Institutes on Aging (R01 AG011378, AG04185) and the Alexander family professorship in Alzheimer's disease research. The data used in this paper are available for download from the ADNI website (http://adni.loni.usc.edu).

Supplementary material

Supplementary material is available at *Brain* online.

References

Agosta F, Pievani M, Geroldi C, Copetti M, Frisoni GB, Filippi M. Resting state fMRI in Alzheimer's disease: beyond the default mode network. Neurobiol Aging 2012; 33: 1564–78.

Andrews-Hanna JR, Reidler JS, Sepulcre J, Poulin R, Buckner RL. Functional-anatomic fractionation of the brain's default network. Neuron 2010; 65: 550–62.

Ashburner J. A fast diffeomorphic image registration algorithm. Neuroimage 2007; 38: 95–113.

Behzadi Y, Restom K, Liau J, Liu TT. A component based noise correction method (CompCor) for BOLD and perfusion based fMRI. Neuroimage 2007; 37: 90–101.

Braak H, Braak E. Neuropathological stageing of Alzheimer-related changes. Acta Neuropathol 1991; 82: 239–59.

Brier MR, Thomas JB, Snyder AZ, Benzinger TL, Zhang D, Raichle ME, et al. Loss of intranetwork and internetwork resting state functional connections with Alzheimer's disease progression. J Neurosci 2012 27; 32: 8890–9.

Buckner RL, Andrews-Hanna JR, Schacter DL. The brain's default network: anatomy, function, and relevance to disease. Ann N Y Acad Sci 2008; 1124: 1–38.

Buckner RL, Sepulcre J, Talukdar T, Krienen FM, Liu H, Hedden T, et al. Cortical hubs revealed by intrinsic functional connectivity: mapping, assessment of stability, and relation to Alzheimer's disease. J Neurosci 2009; 29: 1860–73.

Buldyrev SV, Parshani R, Paul G, Stanley HE, Havlin S. Catastrophic cascade of failures in interdependent networks. Nature 2010; 464: 1025–8.

Bullmore E, Sporns O. Complex brain networks: graph theoretical analysis of structural and functional systems. Nat Rev Neurosci 2009; 10: 186–98.

Calhoun VD, Adali T, Pearlson GD, Pekar JJ. A method for making group inferences from functional MRI data using independent component analysis. Hum Brain Mapp 2001; 14: 140–51.

Crary JF, Trojanowski JQ, Schneider JA, Abisambra JF, Abner EL, Alafuzoff I, et al. Primary age-related tauopathy (PART): a common pathology associated with human aging. Acta Neuropathol 2014; 128: 755–66.

Damoiseaux JS, Prater KE, Miller BL, Greicius MD. Functional connectivity tracks clinical deterioration in Alzheimer's disease. Neurobiol Aging 2012; 33: 828.e19–30.

Dubois B, Feldman HH, Jacova C, Hampel H, Molinuevo JL, Blennow K, et al. Advancing research diagnostic criteria for Alzheimer's disease: the IWG-2 criteria. Lancet Neurol 2014; 13: 614–29.

Elman JA, Oh H, Madison CM, Baker SL, Vogel JW, Marks SM, et al. Neural compensation in older people with brain amyloid-beta deposition. Nat Neurosci 2014; 17: 1316–18.

Erhardt EB, Rachakonda S, Bedrick EJ, Allen EA, Adali T, Calhoun VD. Comparison of multi-subject ICA methods for analysis of fMRI data. Hum Brain Mapp 2011; 32: 2075–95.

Filippini N, MacIntosh BJ, Hough MG, Goodwin GM, Frisoni GB, Smith SM, et al. Distinct patterns of brain activity in young carriers of the APOE-epsilon4 allele. Proc Natl Acad Sci USA 2009; 106: 7209–14.

Greicius MD, Kimmel DL. Neuroimaging insights into network-based neurodegeneration. Curr Opin Neurol 2012; 25: 727–34.

Greicius MD, Srivastava G, Reiss AL, Menon V. Default-mode network activity distinguishes Alzheimer's disease from healthy aging: evidence from functional MRI. Proc Natl Acad Sci USA 2004; 101: 4637–42.

Hallquist MN, Hwang K, Luna B. The nuisance of nuisance regression: spectral misspecification in a common approach to resting-state fMRI preprocessing reintroduces noise and obscures functional connectivity. Neuroimage 2013; 82:208–25.

Iacono D, Markesbery WR, Gross M, Pletnikova O, Rudow G, Zandi P, et al. The Nun study: clinically silent AD, neuronal hypertrophy, and linguistic skills in early life. Neurology 2009; 73: 665–73.

Jack CR Jr, Knopman DS, Jagust WJ, Petersen RC, Weiner MW, Aisen PS, et al. Tracking pathophysiological processes in Alzheimer's disease: an updated hypothetical model of dynamic biomarkers. Lancet Neurol 2013; 12: 207–16.

Jagust WJ, Landau SM. Apolipoprotein E, not fibrillar beta-amyloid, reduces cerebral glucose metabolism in normal aging. J Neurosci 2012; 32: 18227–33.

Jagust WJ, Mormino EC. Lifespan brain activity, beta-amyloid, and Alzheimer's disease. Trends Cogn Sci 2011; 15: 520–6.

Jo HJ, Gotts SJ, Reynolds RC, Bandettini PA, Martin A, Cox RW, et al. Effective preprocessing procedures virtually eliminate distance-dependent motion artifacts in resting state FMRI. J Appl Math 2013; 2013: Article ID 935154.

Jones DT, Machulda MM, Vemuri P, McDade EM, Zeng G, Senjem ML, et al. Age-related changes in the default mode network are more advanced in Alzheimer disease. Neurology 2011; 77: 1524–31.

Jones DT, Vemuri P, Murphy MC, Gunter JL, Senjem ML, Machulda MM, et al. Non-stationarity in the "resting brain's" modular architecture. PLoS One 2012; 7: e39731.

Joshi AD, Pontecorvo MJ, Clark CM, Carpenter AP, Jennings DL, Sadowsky CH, et al. Performance characteristics of amyloid PET with florbetapir F 18 in patients with Alzheimer's disease and cognitively normal subjects. J Nucl Med 2012; 53: 378–84.

Knopman DS, Jack CR Jr, Wiste HJ, Lundt ES, Weigand SD, Vemuri P, et al. 18F-fluorodeoxyglucose positron emission tomography, aging, and apolipoprotein E genotype in cognitively normal persons. Neurobiol Aging 2014; 35: 2096–106.

Machulda MM, Jones DT, Vemuri P, McDade E, Avula R, Przybelski S, et al. Effect of APOE epsilon4 status on intrinsic network connectivity in cognitively normal elderly subjects. Arch Neurol 2011; 68: 1131–6.

Mesulam NM. Neuroplasticity failure in Alzheimer's disease: bridging the gap between plaques and tangles. Neuron 1999; 24: 521–9.

Minoshima S, Giordani B, Berent S, Frey KA, Foster NL, Kuhl DE. Metabolic reduction in the posterior cingulate cortex in very early Alzheimer's disease. Ann Neurol 1997; 42: 85–94.

Mormino EC, Smiljic A, Hayenga AO, Onami SH, Greicius MD, Rabinovici GD, et al. Relationships between beta-amyloid and functional connectivity in different components of the default mode network in aging. Cereb Cortex 2011; 21: 2399–407.

Perez-Nievas BG, Stein TD, Tai HC, Dols-Icardo O, Scotton TC, Barroeta-Espar I, et al. Dissecting phenotypic traits linked to human resilience to Alzheimer's pathology. Brain 2013; 136 (Pt 8): 2510–26.

Petersen RC, editor. Mild cognitive impairment: aging to Alzheimer's disease. New York, NY: Oxford University Press; 2003.

Power JD, Barnes KA, Snyder AZ, Schlaggar BL, Petersen SE. Spurious but systematic correlations in functional connectivity MRI networks arise from subject motion. Neuroimage 2012; 59: 2142–54.

Raichle ME. The brain's default mode network. Annu Rev Neurosci 2015; 38: 433–47.

Raj A, Kuceyeski A, Weiner M. A network diffusion model of disease progression in dementia. Neuron 2012; 73: 1204–15.

Saper CB, Wainer BH, German DC. Axonal and transneuronal transport in the transmission of neurological disease: potential role in system degenerations, including Alzheimer's disease. Neuroscience 1987; 23: 389–98.

Scahill RI, Schott JM, Stevens JM, Rossor MN, Fox NC. Mapping the evolution of regional atrophy in Alzheimer's disease: unbiased analysis of fluid-registered serial MRI. Proc Natl Acad Sci USA 2002; 99: 4703–7.

Seeley WW, Crawford RK, Zhou J, Miller BL, Greicius MD. Neurodegenerative diseases target large-scale human brain networks. Neuron 2009; 62: 42–52.

Sheline YI, Morris JC, Snyder AZ, Price JL, Yan Z, D'Angelo G, et al. APOE4 allele disrupts resting state fMRI connectivity in the absence of amyloid plaques or decreased CSF A{beta}42. J Neurosci 2010; 30: 17035–40.

Spires-Jones TL, Hyman BT. The intersection of amyloid beta and tau at synapses in Alzheimer's disease. Neuron 2014; 82: 756–71.

Song Z, Insel PS, Buckley S, Yohannes S, Mezher A, Simonson A, et al. Brain amyloid-beta burden is associated with disruption of intrinsic functional connectivity within the medial temporal lobe in cognitively normal elderly. J Neurosci 2015; 35: 3240–7.

Sperling RA, Dickerson BC, Pihlajamaki M, Vannini P, LaViolette PS, Vitolo OV, et al. Functional alterations in memory networks in early Alzheimer's disease. Neuromolecular Med 2010; 12: 27–43.

Thal DR, Rub U, Orantes M, Braak H. Phases of A beta-deposition in the human brain and its relevance for the development of AD. Neurology 2002; 58: 1791–800.

Tzourio-Mazoyer N, Landeau B, Papathanassiou D, Crivello F, Etard O, Delcroix N, et al. Automated anatomical labeling of activations in SPM using a macroscopic anatomical parcellation of the MNI MRI single-subject brain. Neuroimage 2002; 15: 273–89.

Ugurbil K, Xu J, Auerbach EJ, Moeller S, Vu AT, Duarte-Carvajalino JM, et al. Pushing spatial and temporal resolution for functional and diffusion MRI in the Human Connectome Project. Neuroimage 2013; 80: 80–104.

Van Essen DC. A population-average, landmark- and surface-based (PALS) atlas of human cerebral cortex. Neuroimage 2005; 28: 635–62.

Warren JD, Fletcher PD, Golden HL. The paradox of syndromic diversity in Alzheimer disease. Nat Rev Neurol 2012; 8: 451–64.

Warren JD, Rohrer JD, Schott JM, Fox NC, Hardy J, Rossor MN. Molecular nexopathies: a new paradigm of neurodegenerative disease. Trends Neurosci 2013; 36: 561–9.

Whitwell JL, Jones DT, Duffy JR, Strand EA, Machulda MM, Przybelski SA, et al. Working memory and language network dysfunction in logopenic aphasia: a task-free fMRI comparison to Alzheimer's dementia. Neurobiol Aging 2015; 36: 1245–52.

Wood SN. Generalized additive models: an introduction with R. Boca Raton: Chapman & Hall/CRC; 2006.

Zhou J, Gennatas ED, Kramer JH, Miller BL, Seeley WW. Predicting regional neurodegeneration from the healthy brain functional connectome. Neuron 2012; 73: 1216–27.